A Simple Model for Deglacial Meltwater Pulses

Alexander A. Robel[1,2], **Victor C. Tsai**[1]

[1]Division of Geological and Planetary Sciences, California Institute of Technology
[2]School of Earth and Atmospheric Sciences, Georgia Institute of Technology

Key Points:

- A simple model can reproduce the approximate timing and amplitude of Meltwater Pulse 1A
- Deglacial meltwater pulses can occur in any ice sheet that has an ice saddle and a height-mass balance feedback
- The amplitude and timing of meltwater pulses is primarily set by climate warming rate and the relative size of deglaciating ice sheets

PLEASE NOTE: THIS ARTICLE IS A POSTPRINT OF A PEER-REVIEWED MANUSCRIPT PUBLISHED AT GEOPHYSICAL RESEARCH LETTERS. DOI: 10.1029/2018GL080884.

Corresponding author: Alexander A. Robel, `robel@caltech.edu`

Abstract

Evidence from radiocarbon dating and complex ice sheet modeling suggests that the fastest rate of sea level rise in Earth's recent history coincided with collapse of the ice saddle between the Laurentide and Cordilleran ice sheets during the last deglaciation. In this study, we derive a simple, two-equation model of two ice sheets intersecting in an ice saddle. We show that two conditions are necessary for producing the acceleration in ice sheet melt associated with meltwater pulses: the positive height-mass balance feedback and an ice saddle geometry. The amplitude and timing of meltwater pulses is sensitively dependent on the rate of climate warming during deglaciation and the relative size of ice sheets undergoing deglaciation. We discuss how simulations of meltwater pulses can be improved and the prospect for meltwater pulses under continued climate warming.

1 Introduction

Past transitions from glacial to interglacial periods were punctuated by meltwater pulse events during which the rate of sea level rise significantly accelerated. Meltwater Pulse 1A (MWP 1A) was one such event (~14.6 kyr before present), when global sea levels rose by 10-20 meters in less than 500 years, constituting the fastest reliably-constrained period of sea level rise in recent geologic history [*Fairbanks*, 1989; *Deschamps et al.*, 2012; *Lambeck et al.*, 2014]. Though there is debate regarding the partitioning of sea level rise associated with MWP 1A between melting of the North American and Antarctic ice sheets [*Clark et al.*, 2002; *Bentley et al.*, 2014], existing geological constraints are consistent with some contribution from rapid melting of the North American ice sheets [*Gomez et al.*, 2015; *Liu et al.*, 2016]. Radiocarbon dates [*Dyke*, 2004; *Carlson and Clark*, 2012] also indicate that the rapid sea level rise of MWP 1A coincides with the opening of an ice-free corridor between the Laurentide and Cordilleran ice sheets, though the amount of ice melt required to open this ice-free corridor is poorly constrained.

Weertman [1961] first showed that a positive feedback between ice sheet height and surface melting intensity can drive deglaciation through a "small ice sheet instability". Though this instability has also been simulated in realistic ice sheet models [*Pollard and DeConto*, 2005; *Abe-Ouchi et al.*, 2013], it is not necessarily accompanied by rapid sea level rise. *Gregoire et al.* [2012] first showed that simulated intense surface melting in the ice saddle region between the Laurentide and Cordilleran ice sheets is associated with a brief acceleration in deglacial sea level rise. Subsequent studies [*Tarasov et al.*, 2012; *Abe-Ouchi et al.*, 2013; *Heinemann et al.*, 2014; *Gregoire et al.*, 2016; *Stuhne and Peltier*, 2017] have simulated similar ice saddle collapse events during the deglaciation of the Laurentide and Cordilleran ice sheets, though the timing, duration and amplitude of the associated meltwater pulses varies significantly between models and does not always match observational constraints. Nonetheless, the broad similarities of simulated meltwater pulses across these complicated models indicate that there are fundamental causes of meltwater pulses that are captured even in coarse ice sheet models. Nonetheless, it is unclear why meltwater pulses tend to occur during the deglaciation of ice saddles, and the role of specific physical processes in setting the characteristics of meltwater pulses.

In this study, we describe a minimal model of two ice sheets that may intersect in an ice saddle. Under idealized climate forcing, this model simulates deglacial meltwater pulses which approximately match the amplitude and timing of observationally-constrained estimates for MWP 1A. The modeled meltwater pulses are caused by the rapid expansion and intensification of surface melt over the ice saddle region, which will occur in any ice sheet with an ice saddle and the height-mass balance feedback. We show that the amplitude and timing of meltwater pulses are largely controlled by the rate of climate warming during deglaciation and the relative volumes of the two deglaciating ice sheets.

2 Model Justification and Derivation

The purpose of this study is to understand how deglaciation occurs under a gradually warming climate when an ice sheet has a saddle geometry and ice surface melt rate is a function of elevation. We formulate our objective in this form because more complex models [*Gregoire et al.*, 2012; *Tarasov et al.*, 2012; *Abe-Ouchi et al.*, 2013; *Ziemen et al.*, 2014; *Heinemann et al.*, 2014] indicate that: (1) there was an ice saddle between the Laurentide and the Cordilleran ice sheets at the Last Glacial Maximum (LGM) and during the early part of the last deglaciation, (2) surface mass balance increased with elevation (to a point), and (3) equilibrium line altitude increased approximately linearly over time during the deglaciation. Understanding the cause of these conditions is interesting (and discussed in the studies cited above), but modeling the complexities of climate and ice flow that produce them are ultimately not the purpose of this study. The model that we derive in this section is self-consistent given these conditions (and others discussed in this section), but in reality these conditions are themselves the result of processes not considered here.

We consider two land-based ice sheets (schematic in Figure 1). The inner sections of both ice sheets are on a flat continental interior (at elevation d_0), and may intersect. The outer sections are on sloping continental margins (with bed slopes s_1 and s_2). This bed geometry is a simple, idealized version of the continental geometry of North America or Greenland. As was originally shown by *Weertman* [1961], horizontal variation in either bed elevation or surface mass balance profile is necessary for the existence of a finite steady-state ice sheet configuration. In this section, we derive a simple model of the evolution of each ice sheet's volume driven by ice sheet surface melting and accumulation.

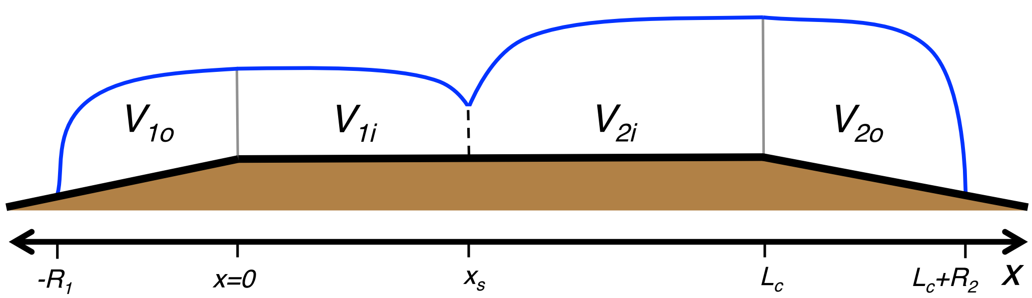

Figure 1. Schematic of model configuration with two ice sheets intersecting. Brown shaded region is bed topography. Blue line is ice sheet surface. Black dashed line indicates ice saddle location (x_s). Grey solid lines indicates locations of ice sheet centers.

2.1 Ice Sheet Elevation

The elevation of the ice sheet surface (E) is the sum of bed elevation and ice sheet thickness. Each ice sheet (labelled with index $j = [1, 2]$) has a generic thickness profile [similar to *Nye*, 1951, 1959] that decreases with distance from the ice sheet maximum

$$h_1(x) = A_1 (R_1 - |x|)^\alpha \tag{1}$$

$$h_2(x) = A_2 (R_2 - |L_c - x|)^\alpha \tag{2}$$

where A_j and α are parameters which set the shape of the ice sheet profile, and R_j is the ice sheet radius from ice thickness maximum to margin. The simplicity of this model is facilitated by the parameterization of ice sheet processes into these few parameters, leaving the ice sheet extents, R_j, as the only prognostic variables. The distance between the two ice sheet maxima is prescribed as L_c, though the model is, in principle, extendable to an arbitrary number of ice sheets.

The saddle point, x_s, is the location at which the two ice sheets intersect (equations 1 and 2 are equal),

$$x_s = \gamma \left[\left(\frac{A_1}{A_2} \right)^{\frac{1}{\alpha}} R_1 - R_2 + L_c \right], \tag{3}$$

where $\gamma = \left[1 + \left(\frac{A_1}{A_2} \right)^{\frac{1}{\alpha}} \right]^{-1}$ is a parameter that measures the asymmetry in ice sheet size parameters. When the ice sheets are separated, the saddle point location for each ice sheet (x_{sj}) is set to the ice sheet extent (see supporting information).

Our assumption of a symmetric ice sheet profile is an approximation based on our idealized choice of bed topography, but could be loosened if the ice sheets had different extents (R_j) in the inner and outer continental section (doubling the number of prognostic variables). Additionally, we prescribe L_c under the assumption [*Gregoire et al.*, 2012, supported by more complex models like] that the ice divides do not migrate significantly during deglaciation and are set primarily by topography and climatic factors. Though future studies may consider the influence of ice divide migration on deglaciation with the advent of efficient high-order ice flow models, such effects are beyond the scope of our simple model.

2.2 Surface Mass Balance

Land-based ice sheets gain and lose mass entirely through accumulation and melting at the ice sheet surface. The surface mass balance (SMB; accumulation minus surface melting) is affected by climatic and ice sheet surface processes over polar ice sheets [*Jenson et al.*, 1996; *Cutler et al.*, 2000], which tend to produce SMB that increases with elevation (E) until reaching a constant

$$M(E) = \begin{cases} a_0 + \beta E & \text{if } E < E_R \\ a_0 + \beta E_R & \text{if } E \geq E_R \end{cases} \tag{4}$$

where a_0 is the sea level SMB, β is the SMB gradient, and E_R is the saturation elevation where SMB becomes constant. The equilibrium line altitude (ELA) is the elevation at which SMB is zero. For simplicity, we apply this SMB function to both ice sheets.

The evolution of each ice sheet's volume is driven by the SMB (equation 4) at the surface of each ice sheet. We take the integral of SMB (equation 4 summed in parts separately above and below E_R) over the ice sheet surface to give an integrated SMB for the inner and outer ice sheet sections

$$B_{jo} = (a_0 + \beta d_0) R_j - \frac{1}{2} \beta s_j \left(R_j^2 - x_{R_j}^2 \right) + \frac{\beta A_j}{\alpha + 1} \left(R_j - x_{R_j} \right)^{\alpha+1} + \beta x_{R_j} \left(E_R - d_0 \right) \tag{5}$$

$$B_{ji} = \beta d_0 \left(x_{sj} - x_{R_j} \right) + \frac{\beta A_j}{\alpha + 1} \left[\left(R_j - x_{R_j} \right)^{\alpha+1} - \left(R_j - x_{sj} \right)^{\alpha+1} \right] + \beta E_R x_{R_j} + a_0 x_{sj} \tag{6}$$

The location of saturation, x_{R_j}, is the horizontal location where $E = E_R$. Under certain circumstances, we can solve for x_{R_j} analytically, and otherwise we use a root-finding method to solve for x_{R_j}. When the runoff line elevation is lower than the ice sheet saddle point elevation, the location of saturation is set to the saddle point location (x_{sj}), and when the runoff line is higher than the entire ice sheet, the location of saturation is set to the ice sheet center. Further details can be found in the supporting information.

2.3 Complete Ice Saddle Model

Ice sheet evolution is described by time derivatives of ice sheet volume (given explicitly in the supporting information), driven by integrated SMB

$$\frac{d}{dt}\left(V_{1o}+V_{1i}\right) = A_1 L_n\left[\left(2R_1^\alpha-\gamma^{\alpha+1}\phi^\alpha\right)\frac{dR_1}{dt}-\gamma^{\alpha+1}\phi^\alpha\frac{dR_2}{dt}\right] = B_{1o}+B_{1i} \quad (7)$$

$$\frac{d}{dt}\left(V_{2o}+V_{2i}\right) = A_2 L_n\left[-\left(1-\gamma\right)^{\alpha+1}\phi^\alpha\frac{dR_1}{dt}+\left(2R_2^\alpha-\left(1-\gamma\right)^{\alpha+1}\phi^\alpha\right)\frac{dR_2}{dt}\right] = B_{2o}+B_{2i} \quad (8)$$

where L_n is the ice sheet extent in the direction perpendicular to ice sheet intersection (in-page in Figure 1), which we assume to be constant. ϕ is the extent of ice sheet overlap: $\phi=\max[R_1+R_2-L_c,0]$. Separating derivatives, we have our simple model

$$\frac{dR_1}{dt} = \left(k_{11}k_{22}-k_{12}k_{21}\right)^{-1}\left[k_{22}\left(B_{1o}+B_{1i}\right)+k_{12}\left(B_{2o}+B_{2i}\right)\right] \quad (9)$$

$$\frac{dR_2}{dt} = \left(k_{11}k_{22}-k_{12}k_{21}\right)^{-1}\left[k_{21}\left(B_{1o}+B_{1i}\right)+k_{11}\left(B_{2o}+B_{2i}\right)\right] \quad (10)$$

where

$$k_{11} = A_1 L_n\left(2R_1^\alpha-\gamma^{\alpha+1}\phi^\alpha\right) \quad (11)$$

$$k_{12} = A_1 L_n\gamma^{\alpha+1}\phi^\alpha \quad (12)$$

$$k_{21} = A_2 L_n\left(1-\gamma\right)^{\alpha+1}\phi^\alpha \quad (13)$$

$$k_{22} = A_2 L_n\left(2R_2^\alpha-\left(1-\gamma\right)^{\alpha+1}\phi^\alpha\right). \quad (14)$$

This model simplifies the complex dynamics of two interacting ice sheets into a system of two strongly nonlinear ordinary differential equations with relatively few parameters.

To derive this simple model of deglacial meltwater pulses, it is necessary to neglect processes which we consider to be less important in a deglaciating ice sheet. Consistent with previous simple models [*Nye*, 1951; *Vialov*, 1958], we assume that each ice sheet profile instantaneously adjusts to changes in surface mass balance over its own surface through unresolved ice flow. Interaction between the two ice sheets only occurs through migration of ice saddle location, though the shape of the ice sheet profiles are unaffected by the presence of the ice saddle. To produce an ice saddle geometry requires that either: (1) SMB in the saddle region is lower than the surrounding regions, or (2) there is a significant out-of-plane ice outflow from the saddle region. Since SMB is typically (and in our model) constant at high elevations (see section 2.2), it is more likely that ice outflow from the saddle is responsible for producing the saddle geometry. Indeed, the Laurentide-Cordillera ice saddle was probably the result of outflow through an ice stream occupying the Mackenzie River trough [*Margold et al.*, 2015]. Despite this out-of-plane flow likely being important for setting the saddle geometry, it can be ignored for the purposes of understanding deglaciation as long as it does not change significantly during this time. Since previous more realistic models [*Tarasov et al.*, 2012; *Gregoire et al.*, 2012] suggest this to be the case, we ignore this potential contribution to deglaciation, and focus entirely on in-plane changes in surface mass balance and ice sheet size. Consequently, our simple model maintains both the prescribed shape of the ice saddle profile and out-of-plane ice sheet extent (L_n) during deglaciation. Such assumptions and simplifications allows us to conduct controlled experiments on the role of ice saddle geometry and surface mass balance in producing deglacial meltwater pulses, which would be more difficult to conduct in models with many more parameters and interdependent degrees of freedom.

3 Necessary Conditions for a Meltwater Pulse

Meltwater pulses occurred (among other times) during deglacial periods of increasing atmospheric temperature. We reproduce this climatic forcing by assuming a linear trend in the SMB at sea level

$$a_0(t) = a_0(t = 0) - a_{tr}t. \tag{15}$$

In this section, we use a deglacial SMB trend similar to those simulated in complex climate models [e.g. *Gregoire et al.*, 2016]. This trend is applied to a two-ice sheet configuration, initialized at a steady-state, attained by setting other model parameters (listed in caption of Figure 2) to realistic values which produce an ice sheet with geometry comparable to the Laurentide-Cordilleran saddle region during the LGM.

The simulated deglaciation of two intersecting ice sheets under a warming climate is plotted in Figure 2. After the onset of warming, there is a gradual expansion and intensification of surface melt in the outer ice sheet regions, while the inner saddle region maintains a constant positive surface mass balance (Figure 2b). Approximately 3000 years after the onset of deglaciation (solid grey line in Figure 2c), there is an acceleration in the rate of melting in the ice sheet interior when the ELA reaches the elevation of the ice saddle, and which we identify as a meltwater pulse. Acceleration in interior surface melting is driven by two processes. The first process is the height-mass balance feedback, which causes surface melting to intensify as the saddle lowers in elevation (red line becomes more negative in Figure 2c). The second process is the rapid expansion of the interior ice sheet area that is experiencing surface melting (blue line increases in Figure 2c). The interior melt area expands rapidly due to the geometry of the ice saddle (set, in part, by α). The product of the height-mass balance feedback and the expansion of interior melt area (i.e. the volumetric rate of interior surface melt) explains the initial superlinear rate of acceleration in the ice sheet melt rate.

Gregoire et al. [2012] first identified the height-mass balance feedback within the ice saddle region as an important process in their simulation of MWP 1A. The simulation in their study provides a single scenario in which a meltwater pulse is generated. Our simple model allows us to generalize this result to determine the minimally necessary conditions under which meltwater pulses occur (including MWP 1A). In the supporting information we compare the simulation plotted in Figure 2 to an equivalent simulation with a single ice sheet (and the height-mass balance feedback built-in). In contrast to the simulation with two ice sheets, a single ice sheet does not produce a meltwater pulse-like acceleration in ice loss rate because surface melting occurring on both ice sheet flanks (in the absence of an ice saddle) is determined entirely by the forcing (linear climate warming). Additionally, in the absence of a height-mass balance feedback in the ice sheet interior, there would be no increase in surface melt area or intensity to produce the meltwater pulse in the first place. Our simple model demonstrates the general principle [of which *Gregoire et al.*, 2012, is one example] that meltwater pulses require: (1) the height-mass balance feedback, and (2) an ice saddle geometry. In identifying these necessary necessary conditions for meltwater pulses, we are translating what has been learned about past ice sheet dynamics (i.e. MWP 1A) to identify other ice sheets and scenarios in which meltwater pulses might occur again.

The second phase of the meltwater pulse begins approximately 4400 years after the onset of deglaciation (dashed grey line in Figure 2c), when the ice sheets separate and acceleration in the rate of ice sheet melt slows due to a decrease in the area of interior melting (blue line in Figure 2c). During this second phase of the meltwater pulse, the "minor" ice sheet (i.e. the smaller of the two ice sheets) is undergoing the small ice sheet instability [*Weertman*, 1961] through an expansion in the area of ice surface melt (blue line in Figure 2c).

The meltwater pulse terminates approximately 5600 years after the onset of deglaciation (dotted grey line in Figure 2c), when the minor ice sheet disappears. Following the meltwater pulse, the "major" ice sheet continues to deglaciate through continuing intensification of the rate of surface melt, though over a dwindling area. The concomittent intensification of surface melting and decrease in area of surface melting make for a rel-

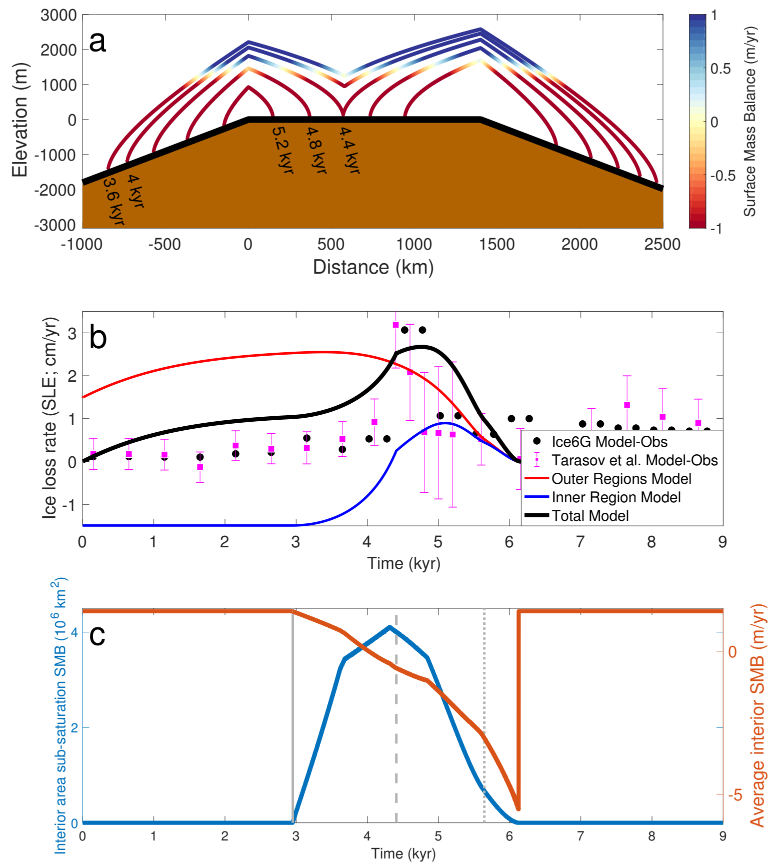

Figure 2. Simulation of a Laurentide-like deglacial meltwater pulse. (a) Ice sheet elevation profile during meltwater pulse, with colors indicating surface mass balance and labels indicating time of profile. (b) Rate of ice volume loss as a function of time (in cm/yr sea level equivalent; SLE). Red and blue lines are total simulated volume loss rate on outer and inner regions of ice sheets, respectively (see Figure 1). Black line is total simulated volume loss rate over both ice sheets. Black circles are observationally-constrained estimates of ice volume loss rate from the Laurentide-Cordilleran Ice Sheet complex from *Peltier et al.* [2015]. Purple squares are from a model-data estimate of ice volume loss rate from the Laurentide-Cordilleran Ice Sheet complex from *Tarasov et al.* [2012] (the N5a ensemble with 1-sigma uncertainty estimates). For both sets of observations, $x = 0$ kyr corresponds to 18.7 kyr before present. (c) Blue line is the area of the simulated inner ice sheet region below saturation SMB as a function of time. Red line is the simulated average SMB in over inner ice sheet regions as a function of time. Grey lines indicate important events during the meltwater pulse: solid - onset of sub-saturation SMB in interior, dashed - separation of ice sheets, dotted - disappearance of minor ice sheet. Parameters used in simulation: $\alpha = \frac{1}{2}$, $A_1 = 2.4$ meters$^{\frac{1}{2}}$, $A_2 = 2.5$ meters$^{\frac{1}{2}}$, $L_c = 1400$ kilometers, $L_n = 3500$ kilometers, $d_0 = 0$ meters, $\beta = 3 \times 10^{-3}$ 1/yr, $s_1 = s_2 = 1.8 \times 10^{-3}$, $a_0(t = 0) = -1$ meters/year, $H_R = 800$ meters, $a_{tr} = 7.5 \times 10^{-4}$ meters/year^2.

atively "smooth" final deglaciation, in line with simulations of single ice sheet deglaciation through the small ice sheet instability (see single ice dome deglacial simulations in the supporting information).

Two independent observationally-constrained volume loss rates for the Laurentide-Cordilleran ice sheets are plotted in Figure 2b, derived from the ICE-6G estimate [black circles; *Peltier et al.*, 2015] and *Tarasov et al.* [2012] (purple squares). We show this comparison between the simple model and observations to point out that our simple model can approximately reproduce the timing, duration and amplitude of MWP 1A observations, taking into account the significant uncertainties associated with such observational estimates [see 1-sigma uncertainty estimates from *Tarasov et al.*, 2012]). The observations do suggest that the rate of ice sheet melting early in deglaciation was generally lower than is simulated in the simple model, and the acceleration associated with MWP 1A was sharper than our simulations. However, it is inadvisable to attempt to "validate" the model by making such a detailed comparison to observations, due partly to the simplicity of the model and partly to the poor observational constraints on MWP 1A. This simple model is a useful tool for understanding the conditions under which meltwater pulses occur and their dependence on ice sheet and forcing parameters.

4 Amplitude and Timing of Meltwater Pulses

The amplitude and timing of meltwater pulses simulated with complex 3D ice sheet models [*Gregoire et al.*, 2012; *Abe-Ouchi et al.*, 2013; *Heinemann et al.*, 2014] differ significantly between models, and often are in disagreement with observationally-determined sea level records. In models that are parametrically tuned to match records of sea level and ice sheet extent [*Tarasov et al.*, 2012; *Gregoire et al.*, 2016; *Stuhne and Peltier*, 2017], the agreement is better (by design), but the particular physical processes controlling the characteristics of meltwater pulses is unclear. In this section, we show how the parameters and initial conditions in our simple model set the amplitude and timing of meltwater pulses.

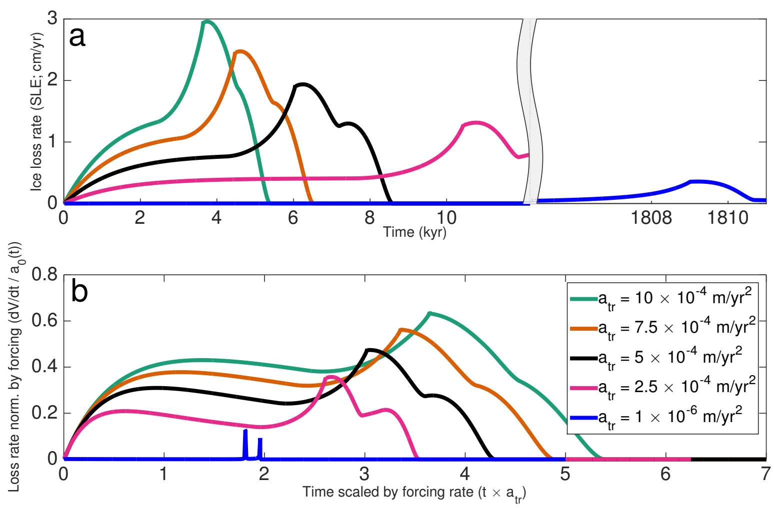

Figure 3. Meltwater pulse properties as a function of forcing rate. (a) Ice loss rate as a function of time for different warming rates (a_{tr}). Orange line is identical to the simulation plotted in Figure 2. X-axis is broken to show the transient quasi-equilibrium simulation (blue line). (b) Normalized ice loss rate as a function of scaled time. Y-axis is the ice loss rate divided by the time-dependent sea level SMB ($a_0(t)$). X-axis is time multiplied by the rate of forcing (a_{tr}). All parameter values, except a_{tr}, are the same as those used in Figure 2.

The prescribed rate of deglacial climate warming has a strong influence on the amplitude and timing of meltwater pulses. Figure 3 compares five meltwater pulses simulated in the simple model, with varying rates of climate warming (a_{tr} in equation 15). Faster warming causes the ELA to reach the ice saddle elevation earlier, leading to an earlier meltwater pulse (Figure 3a). However, scaling time by the rate of climate warming (x-axis of Figure 3b) shows that the meltwater pulse tends to occurs later than would be explained by the warming rate alone. The ice sheet volume and ice saddle elevation take a finite length of time to equilibrate to ongoing warming. Consequently, for faster climate warming, the intensity of surface melting and the total ice sheet volume are higher at the onset of the meltwater pulse, leading to a meltwater pulse with greater amplitude. We also normalize the ice loss rate by the time-evolving forcing (y-axis of Figure 3b). The meltwater pulse amplitude is greater than would be explained by the SMB at the time of the meltwater pulse alone, indicating that the ice sheet size at the time of the meltwater pulse is equally important in setting the meltwater pulse amplitude.

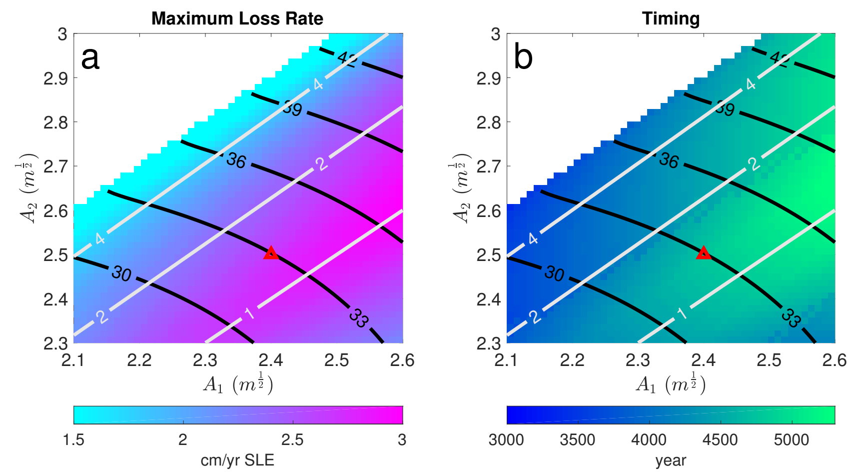

Figure 4. Meltwater pulse properties as a function of ice sheet size parameters. (a) Maximum rate of ice loss during meltwater pulse in cm/yr sea level equivalent. (b) Timing of meltwater pulse after onset of climate forcing in years. In both panels, x- and y- axes are ice sheet size parameters A_1 and A_2, respectively. Red triangle marks location of simulation shown in Figure 2. Black contours are total volume of both ice sheets in pre-meltwater pulse steady-state configuration (in units of 10^6 km^3). Grey contours are ratio of ice sheet 2 volume to ice sheet 1 volume. Laurentide-Cordilleran Ice Sheet complex volume was 33×10^6 km^3 during the LGM [based on ICE-6G estimate, see *Peltier et al.*, 2015]. Simulations in region shaded in white do not include a meltwater pulse.

We determine the proportion of the meltwater pulse amplitude that is explained by forcing rate (as opposed to internal ice sheet melting dynamics) by comparing simulations with warming rates comparable to the last deglaciation (a_{tr}~10^{-3} m/yr^2) to a quasi-equilibrium simulation with a very slow warming rate ($a_{tr} = 10^{-6}$ m/yr^2; blue line Figure 3). The amplitude of the meltwater pulse in the quasi-equilibrium simulation is set by the difference between the smallest steady-state ice volume with two ice sheets and the largest steady-state ice volume with zero ice sheets (i.e. the saddle-node bifurcation between the model's two equilibria, see bifurcation diagram in supporting information). With the same parameters and initial configuration as in the simulation shown in Figure 2, the quasi-equilibrium simulation has a meltwater pulse amplitude of ~0.5 cm/yr sea level equivalent (SLE). This amplitude is less than half the meltwater pulse amplitude for the deglacial warming rate simulations, leading to the conclusion that most of the meltwater pulse amplitude is set by the forcing rate at deglacial rates of climate warming.

Many parameters in the simple model have an influence on the initial steady-state configuration of ice sheets, which in turn has a strong influence on the amplitude and timing of simulated meltwater pulses. We plot the amplitude (Figure 4a) and timing (Figure 4b) of simulated meltwater pulses for different combinations of the two ice sheet size parameters, A_1 and A_2. We also plot contours of total ice volume in the pre-meltwater pulse steady-state (in black) and the ratio of ice sheet volumes in the pre-meltwater pulse steady-state (in grey). Perhaps counter-intuitively, it is the relative size of the two ice sheets (and not total initial ice volume) which is the primary determinant of meltwater pulse amplitude and timing. When the two ice sheets are closer in size, the resulting meltwater pulse has a higher amplitude and occurs later in time. When the minor ice sheet is larger, the ELA needed to trigger the small ice sheet instability is higher, causing the meltwater pulse to occur later [*Weertman*, 1961]. When the ice sheets are close in size, more of the deglaciation of the "major" ice sheet occurs during the meltwater pulse, increasing the meltwater pulse amplitude. For a given total ice volume, the largest possible meltwater pulse occurs when the two ice sheets are the same size ($A_1 = A_2$) and lasts until both ice sheets are completely deglaciated. Since our model is symmetric with respect to the two ice sheets, the same meltwater pulse will occur for a given pair of initial ice sheet sizes, regardless of order (i.e. the same meltwater pulse occurs for $[A_1, A_2]$ and $[A_2, A_1]$). Other parameters also influence the amplitude and timing of meltwater pulses through the initial steady-state configuration of ice sheets (see supporting information).

5 Discussion and Implications

We have described a simple model that is capable of producing a meltwater pulse that resembles observations of MWP 1A. In previous simulations of MWP 1A using complex ice sheet models, a meltwater pulse occurs several thousand years later than what is indicated by many independent lines of observation [*Gregoire et al.*, 2012; *Abe-Ouchi et al.*, 2013; *Heinemann et al.*, 2014]. The results of our simple model suggest that such a delayed onset of the simulated meltwater pulse may be caused by either: (a) deglacial climate warming being too slow, or (b) the LGM size of the Cordilleran Ice Sheet being too large relative to the Laurentide Ice Sheet. Possibility (b) also implies that the amplitude of the simulated meltwater pulse is too large (Figure 4a), and the proportion of the observed rise in sea level associated with MWP 1A ascribed to Antarctic melting would necessarily be greater [as discussed in *Gomez et al.*, 2015; *Liu et al.*, 2016]. The opposite is true of possibility (a). As Figure 4 demonstrates, to accurately simulate a deglacial meltwater pulse, it is critically important to match models to observations of the relative volumes of the two intersecting ice sheets, in contrast to some studies [e.g. *Gregoire et al.*, 2016] which match total ice volume to observations. Matching relative ice sheet volumes would likely necessitate the calibration of ice sheet model parameters in a spatially-varying fashion [as in the data-model fusion of *Tarasov et al.*, 2012].

As we state in section 2, we do not seek to determine why ice saddles exist, but rather to determine the implications of a generic ice-saddle geometry (and the height-mass balance feedback) for the evolving rate of ice sheet deglaciation. Geomorphological observations [*Margold et al.*, 2015] suggest that the Laurentide-Cordillera ice saddle was maintained during the LGM by an ice stream occupying the Mackenzie River trough, and that a series of ephemeral ice streams may have appeared in the saddle during deglaciation, potentially aided by the formation of proglacial lakes. Though some studies have coarsely simulated ice stream flow responses to climate warming on paleoclimatic time scales [*Tarasov et al.*, 2012; *Robel and Tziperman*, 2016], even state-of-the-art ice sheet models have difficulty accurately resolving the shear margin and onset zones of ice streams [*Hindmarsh*, 2009; *Haseloff et al.*, 2018], and almost none simulate proglacial lake formation. Though adding more ice sheet processes to our minimal model may produce quantitative changes in simulated meltwater pulses, the inability of current 3D models to properly simulate transient ice stream dynamics on paleoclimate time scales makes it difficult to definitely say whether such changes would alter any of our conclusions, which as we have shown, are fundamentally the consequence of ice sheet geometry and the height-mass balance feedback.

One general implication of our simple model is that any land-based ice sheet with an ice saddle-like geometry (and the height-mass balance feedback) has the potential to produce a meltwater pulse in a warming climate. Indeed, some simulations of the multi-domed Greenland Ice Sheet in warm past climates have raised the possibility of ice saddle collapse in Southeast Greenland [*Ridley et al.*, 2010; *Robinson et al.*, 2011]. However, such studies have typically focused on the equilibrium states of the Greenland Ice Sheet, rather than the transient rate of deglaciation. A future study might focus on how the multi-domed geometry and the internal dynamics of the Greenland Ice Sheet could lead to a meltwater pulse under transient climate warming.

Acknowledgments

A simple numerical implementation of the mathematical model described in this study is available as a public repository on GitHub: https://github.com/aarobel/. This work was primarily supported by the NSF Arctic Natural Sciences Program (Grant OPP 1735715). AAR was also supported by the NOAA Climate and Global Change Postdoctoral Fellowship and the Caltech Stanback Postdoctoral Fellowship during an early phase of this project. Thanks to Lev Tarasov for providing the output from his observationally-constrained Laurentide Ice Sheet model.

References

Abe-Ouchi, A., F. Saito, K. Kawamura, M. E. Raymo, J. Okuno, K. Takahashi, and H. Blatter (2013), Insolation-driven 100,000-year glacial cycles and hysteresis of ice-sheet volume, *Nature*, *500*(7461), 190–193.

Bentley, M. J., C. Ó. Cofaigh, J. B. Anderson, H. Conway, B. Davies, A. G. Graham, C.-D. Hillenbrand, D. A. Hodgson, S. S. Jamieson, R. D. Larter, et al. (2014), A community-based geological reconstruction of Antarctic Ice Sheet deglaciation since the Last Glacial Maximum, *Quaternary Science Reviews*, *100*, 1–9.

Carlson, A. E., and P. U. Clark (2012), Ice sheet sources of sea level rise and freshwater discharge during the last deglaciation, *Reviews of Geophysics*, *50*(4).

Clark, P. U., J. Mitrovica, G. Milne, and M. Tamisiea (2002), Sea-level fingerprinting as a direct test for the source of global meltwater pulse 1A, *Science*, *295*(5564), 2438–2441.

Cutler, P. M., D. R. MacAyeal, D. M. Mickelson, B. R. Parizek, and P. M. Colgan (2000), A numerical investigation of ice-lobe–permafrost interaction around the southern Laurentide ice sheet, *Journal of Glaciology*, *46*(153), 311–325.

Deschamps, P., N. Durand, E. Bard, B. Hamelin, G. Camoin, A. L. Thomas, G. M. Henderson, J. Okuno, and Y. Yokoyama (2012), Ice-sheet collapse and sea-level rise at the bolling warming 14,600 years ago, *Nature*, *483*(7391), 559–564.

Dyke, A. S. (2004), An outline of North American deglaciation with emphasis on central and northern Canada, in *Developments in Quaternary Sciences*, vol. 2, pp. 373–424, Elsevier.

Fairbanks, R. G. (1989), A 17,000-year glacio-eustatic sea level record: influence of glacial melting rates on the Younger Dryas event and deep-ocean circulation, *Nature*, *342*(6250), 637–642.

Gomez, N., L. Gregoire, J. Mitrovica, and A. Payne (2015), Laurentide-Cordilleran Ice Sheet saddle collapse as a contribution to meltwater pulse 1A, *Geophysical Research Letters*, *42*(10), 3954–3962.

Gregoire, L. J., A. J. Payne, and P. J. Valdes (2012), Deglacial rapid sea level rises caused by ice-sheet saddle collapses, *Nature*, *487*(7406), 219–222.

Gregoire, L. J., B. Otto-Bliesner, P. J. Valdes, and R. Ivanovic (2016), Abrupt Bølling warming and ice saddle collapse contributions to the Meltwater Pulse 1a rapid sea level rise, *Geophysical research letters*, *43*(17), 9130–9137.

Haseloff, M., C. Schoof, and O. Gagliardini (2018), The role of subtemperate slip in thermally-driven ice stream margin migration, *The Cryosphere Discussions*, *2018*, 1–30, doi:10.5194/tc-2017-244.

Heinemann, M., A. Timmermann, O. Elison Timm, F. Saito, and A. Abe-Ouchi (2014), Deglacial ice sheet meltdown: Orbital pacemaking and CO_2 effects, *Climate of the Past*, *10*(4), 1567–1579.

Hindmarsh, R. C. A. (2009), Consistent generation of ice-streams via thermo-viscous instabilities modulated by membrane stresses, *Geophysical Research Letters*, *36*, doi:10.1029/2008GL036877.

Jenson, J. W., D. R. MacAyeal, P. U. Clark, C. L. Ho, and J. C. Vela (1996), Numerical modeling of subglacial sediment deformation: Implications for the behavior of the Lake Michigan Lobe, Laurentide Ice Sheet, *Journal of Geophysical Research: Solid Earth*, *101*(B4), 8717–8728.

Lambeck, K., H. Rouby, A. Purcell, Y. Sun, and M. Sambridge (2014), Sea level and global ice volumes from the last glacial maximum to the holocene, *Proceedings of the National Academy of Sciences*, *111*(43), 15,296–15,303.

Liu, J., G. A. Milne, R. E. Kopp, P. U. Clark, and I. Shennan (2016), Sea-level constraints on the amplitude and source distribution of Meltwater Pulse 1A, *Nature Geoscience*, *9*(2), 130–134.

Margold, M., C. R. Stokes, and C. D. Clark (2015), Ice streams in the laurentide ice sheet: Identification, characteristics and comparison to modern ice sheets, *Earth-Science Reviews*, *143*, 117–146.

Nye, J. (1951), The flow of glaciers and ice-sheets as a problem in plasticity, *Proc. R. Soc. Lond. A*, *207*(1091), 554–572.

Nye, J. (1959), The motion of ice sheets and glaciers, *Journal of Glaciology*, *3*(26), 493–507.

Peltier, W., D. Argus, and R. Drummond (2015), Space geodesy constrains ice age terminal deglaciation: The global ICE-6G_C (VM5a) model, *Journal of Geophysical Research: Solid Earth*, *120*(1), 450–487.

Pollard, D., and R. M. DeConto (2005), Hysteresis in cenozoic antarctic ice-sheet variations, *Global and Planetary Change*, *45*(1), 9–21.

Ridley, J., J. M. Gregory, P. Huybrechts, and J. Lowe (2010), Thresholds for irreversible decline of the Greenland ice sheet, *Climate Dynamics*, *35*(6), 1049–1057.

Robel, A. A., and E. Tziperman (2016), The role of ice stream dynamics in deglaciation, *Journal of Geophysical Research: Earth Surface*, *121*(8), 1540–1554.

Robinson, A., R. Calov, and A. Ganopolski (2011), Greenland ice sheet model parameters constrained using simulations of the Eemian Interglacial, *Climate of the Past*, *7*(2), 381–396.

Stuhne, G., and W. Peltier (2017), Assimilating the ICE-6G_C Reconstruction of the Latest Quaternary Ice Age Cycle Into Numerical Simulations of the Laurentide and Fennoscandian Ice Sheets, *Journal of Geophysical Research: Earth Surface*, *122*(12), 2324–2347.

Tarasov, L., A. S. Dyke, R. M. Neal, and W. R. Peltier (2012), A data-calibrated distribution of deglacial chronologies for the North American ice complex from glaciological modeling, *Earth and Planetary Science Letters*, *315*, 30–40.

Vialov, S. (1958), Regularities of glacial shields movement and the theory of plastic viscous flow, *International Association of Hydrological Sciences Publications*, *47*, 266–275.

Weertman, J. (1961), Stability of ice-age ice sheets, *Journal of Geophysical Research*, *66*(11), 3783–3792.

Ziemen, F., C. Rodehacke, and U. Mikolajewicz (2014), Coupled ice sheet–climate modeling under glacial and pre-industrial boundary conditions, *Climate of the Past*, *10*, 1817–1836.